ADVANCED MATERIALS
www.advmat.de

Blood-Glucose-Powered Metabolic Fuel Cell for Self-Sufficient Bioelectronics

*Debasis Maity, Preetam Guha Ray, Peter Buchmann, Maysam Mansouri, and Martin Fussenegger**

Currently available bioelectronic devices consume too much power to be continuously operated on rechargeable batteries, and are often powered wirelessly, with attendant issues regarding reliability, convenience, and mobility. Thus, the availability of a robust, self-sufficient, implantable electrical power generator that works under physiological conditions would be transformative for many applications, from driving bioelectronic implants and prostheses to programing cellular behavior and patients' metabolism. Here, capitalizing on a new copper-containing, conductively tuned 3D carbon nanotube composite, an implantable blood-glucose-powered metabolic fuel cell is designed that continuously monitors blood-glucose levels, converts excess glucose into electrical power during hyperglycemia, and produces sufficient energy (0.7 mW cm^{-2}, 0.9 V, 50 mM glucose) to drive opto- and electro-genetic regulation of vesicular insulin release from engineered beta cells. It is shown that this integration of blood-glucose monitoring with elimination of excessive blood glucose by combined electro-metabolic conversion and insulin-release-mediated cellular consumption enables the metabolic fuel cell to restore blood-glucose homeostasis in an automatic, self-sufficient, and closed-loop manner in an experimental model of type-1 diabetes.

1. Introduction

Interconnected smart electronic devices are increasingly dominating our daily lives and shaping new opportunities in biomedical sciences.[1,2] While current electronic wearables mainly collect and process basic physical parameters and healthcare data,[3–5] forefront research in bioelectronics has shown that molecular interfaces between cells and electronics can in principle be incorporated into bioelectronic implants that coordinate biomarker monitoring and information processing with the production and release of protein therapeutics by engineered cells.[6–8] Interoperability between biological and electronic systems has been achieved through recent advances in synthetic biology that established programmable genetic circuits capable of implementing electronic control and processing principles,[9] such as oscillators,[10–12] analogue-to-digital converters,[13] and half- and full-adders.[14,15] This has enabled the design of bioelectronic interfaces programming cellular behavior with traceless physical cues powered by electricity,[16] including light,[3,6,17,18] magnetic fields,[19] heat,[20] and direct electrical fields.[7,21]

Stimulation of engineered cells by light,[17] or electrical fields,[7,21] which interface with synthetic signaling cascades controlling cellular membrane depolarization, is particularly attractive for biomedical applications, as such systems can trigger fast vesicular release of biopharmaceuticals within minutes. This is essential for the treatment for medical conditions such as type-1 diabetes that require sophisticated dynamic control.[22–24] Electro-stimulated fast vesicular release is achieved either by activating recombinant retinal melanopsin with blue light,[17,22] or by sensitizing cells to electrical fields by co-expressing the L-type voltage-gated channel $Ca_V1.2$ and the inwardly rectifying potassium channel $K_{ir}2.1$ in human cells.[7]

However, currently available bioelectronics and bioelectronic implants, in particular those based on optogenetics, consume too much power to be continuously operated on rechargeable batteries. They have to be wirelessly powered by extracorporeal field generators linked to a socket outlet, which limits safety, convenience and mobility.[6,7,21,25] Therefore, the future development of bioelectronics and bioelectronic implants will depend on the availability of a reliable, self-sufficient, implantable electrical power generator.

Circulating body fluids contain a variety of high-energy metabolites that could in principle be harnessed to continuously produce the electrical power required to operate bioelectronics in a self-sufficient manner. A particularly promising

D. Maity, P. Guha Ray, P. Buchmann, M. Mansouri, M. Fussenegger
Department of Biosystems Science and Engineering
ETH Zurich
Mattenstrasse 26, Basel CH-4058, Switzerland
E-mail: fussenegger@bsse.ethz.ch
M. Fussenegger
Faculty of Science
University of Basel
Mattenstrasse 26, Basel CH-4058, Switzerland

The ORCID identification number(s) for the author(s) of this article can be found under https://doi.org/10.1002/adma.202300890.

[+]Present address: Vector BioPharma AG, Hochbergerstrasse 60C, Basel CH-4057, Switzerland

DOI: 10.1002/adma.202300890

substrate seems to be blood glucose, whose postprandial spikes could be available for electro-metabolic conversion. Chronic hyperglycemia associated with diabetes mellitus affects over ten percent of the global population,[26] and therefore could provide a permanent electrical power source for bioelectronics. Furthermore, the continuous dissipation of excess metabolic energy by electro-metabolic conversion might also help in restoring blood-glucose homeostasis.

First-generation glucose-utilizing biofuel cells relying on purified glucose oxidase have indeed established the general principle of electro-metabolic conversion,[27–31] However, low power output, limited electron transfer, poor shelf/half-life of the enzyme, and biofouling of implanted electrodes have so far limited real-world applications.[32] Electron-transfer efficiency and conductance were significantly improved by conjugating the glucose oxidase to 1D nanomaterials such as graphene or multi-walled carbon nanotubes (MWCNTs),[33] but the fact that these biofuel cells consumed oxygen, which promotes hypoxia and electrode corrosion, renders them useless for clinical applications.[34,35] Replacing glucose oxidase with electro-active metal oxides such as cupric oxide (CuO) embedded in 1- or 2D carbon nanocomposites indeed improved the stability, shelf-life and long-term performance, but due to the lower electron transfer rate of glucose electrocatalysis, the power-density of these non-enzymatic glucose biofuel cells is not sufficient to drive bioelectronic implants.[36] Furthermore, the use of free-standing composites and the lack of a biocompatible matrix material for the electrodes has so far prevented the development of clinical applications of non-enzymatic biofuels cells.[33,37–39] However, hybrid enzymatic biofuel cells have recently shown promising performance. For example, biofuel cell fabrication based on glucose-oxidase (GOx)-coated metallic cotton fibers or GOx-loaded carbon cloth (CC) generated power density (PD) of 3.7 mW cm^{-2} and 1.07 mW cm^{-2} in 300 mM and 100 mM glucose solution respectively.[40,41] Further, GOx was also coated on crosslinked CNTs to achieve a PD of 0.94 mW cm^{-2} in 200 mM glucose solution under O_2 saturation.[42] In a parallel study, GOx-loaded organic-metallic composite-based CNT-Ag/napthalenethiol afforded an output PD of 1.46 mW cm^{-2} in the presence of 400 mM glucose.[43] Nevertheless, these enzymatic biofuel cells only work at glucose concentrations of 100 mM or above, considerably above the physiological glucose concentration even under diabetic conditions.

To overcome these issues, we have designed a hierarchically decorated three-dimensional matrix of CuO-MWCNTs and poly(3,4-ethylenedioxythiophene)-poly(styrenesulfonate) (PEDOT:PSS) composite (CuO-MWCNTs-PEDOT:PSS) and fabricated a mediator-free metabolic fuel cell that constantly monitors blood-glucose levels, exclusively produces electricity during hyperglycemia and generates sufficient electricity to power and control optogenetic- as well as electrogenetic-based bioelectronic implants. By programming these bioelectronic implants for rapid release of insulin from engineered human cells using optogenetic or electrogenetic interfaces, we have established closed-loop metabolic control systems that can autonomously restore glucose homeostasis in experimental type-1 diabetes.

2. Results

2.1. Concept of the Metabolic Fuel Cell

We have designed an implantable metabolic fuel cell that plugs into mammalian energy metabolism by catalyzing the conversion of excess blood glucose into non-insulinogenic renally secreted gluconate, thereby releasing an electron and converting metabolic energy into electrical power (**Figure 1**). The electrical power management circuit constantly monitors blood-glucose levels, and connects the metabolic fuel cell to wearable and mobile devices for communication, recording and external tuning. Its low-power boost charger and capacitor, charged during hyperglycemia, provide over 4 volts, which is sufficient to power electrogenetic and optogenetic control of biopharmaceutical production by implanted engineered human cells (Figure 1). Connection of the metabolic fuel cell to electro- or opto-genetic insulin production by engineered human cells produces a closed-loop control circuit in which the metabolic fuel cell is switched ON during hyperglycemia and triggers electro- or opto-genetic rapid release of insulin. The combined effect of glucose consumption by the metabolic fuel cell and insulin-release-mediated cellular glucose uptake restores blood-glucose homeostasis, which switches the metabolic fuel cell OFF to prevent hypoglycemia (Figure 1). Since the blood-glucose level itself adjusts the charge storage of the metabolic fuel cell, diabetes control is achieved in a completely autonomous, self-sufficient, and seamless manner (Figure 1).

2.2. Design of the Metabolic Fuel Cell

The metabolic fuel cell employs flexible interconnected electrodes assembled by 3D monolithic amalgamation of different nanomaterials. The anode consists of a flexible graphite felt, providing 3D support for the spatially decorated CuO-MWCNTs-PEDOT:PSS complex. While Cu(II) to Cu(III) transition of the CuO catalyzes the oxidation of glucose into gluconate, the multi-walled carbon nanotubes capture, remove and transport the resulting electron supported by the conductive filler, PEDOT:PSS (Figures 1, **2**A). The cathode consists of a flexible CC providing 3D support for the carbon black (CB)-decorated platinum nanoparticles (PtNP), which are deep-coated with Nafion to maximize and selectively harness protons from the anode-based glucose-to-gluconate oxidation, enabling platinum-catalyzed reaction of the protons with oxygen to generate H_2O, thus closing the electrical cycle of the metabolic fuel cell (Figures 1, **3**A).

2.3. Characterization and Validation of the Anode

Morphological analysis of the anode by field emission scanning electron microscopy (FESEM) (Figure 2A-i,ii) and transmission electron microscopy (TEM) confirmed the 3D structure consisting of MWCNTs (≈30 nm in width) homogeneously coated with small aggregates of CuO nanoparticles (≈50–150 nm in diameter) and filled with conductive PEDOT:PSS

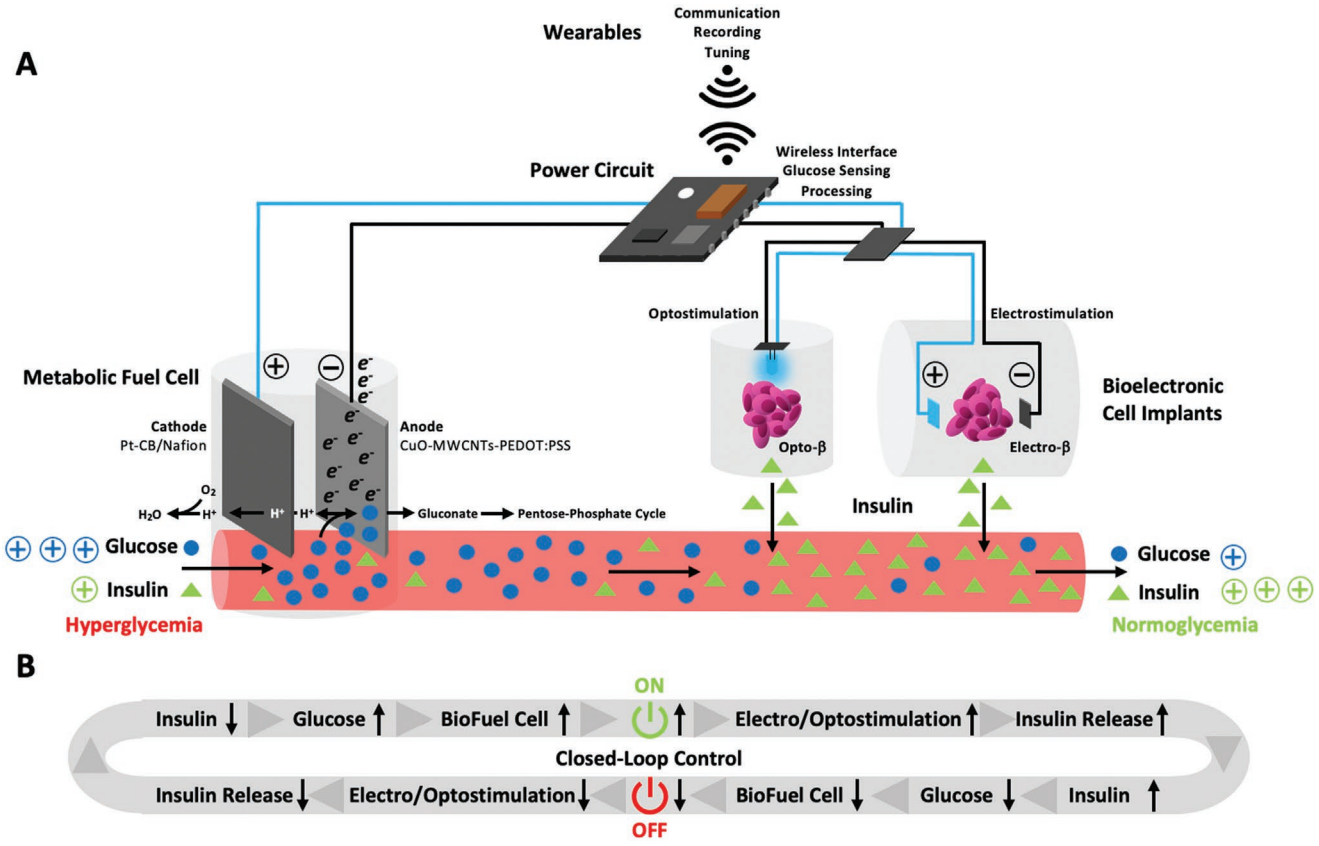

Figure 1. Schematic of the non-enzymatic metabolic fuel cell for closed-loop control of blood-glucose homeostasis. A) Operation of the metabolic fuel cell. After implantation, the metabolic fuel cell connects to the bloodstream. At the anode, consisting of cupric oxide (CuO) nanoparticles embedded into multi-walled carbon nanotubes (MWCNTs) and coated with poly-(3,4-ethylenedioxythiophene)-poly(styrenesulfonate) (PEDOT:PSS) (CuO-MWCNTs-PEDOT:PSS), glucose is catalytically converted to gluconate with concomitant generation of protons (H^+) and electrons (e^-). While gluconate is either renally cleared or enters the pentose-phosphate cycle, the electronic circuit is supplied with the electrons, and the protons travel to the cathode, consisting of Nafion-coated carbon black (CB)-containing platinum (Pt) nanoparticles (Pt-CB/Nafion), where they reduce oxygen to water (H_2O). The electrons travel to the power circuit which provides a wireless interface with wearables for communication, recording and tuning, manages glucose sensing and processes the operation of the metabolic fuel cell at blood-glucose levels above 10 mM glucose. The harnessed electrical energy is used to stimulate engineered human cells to release therapeutic proteins such as insulin in response to light (optostimulation of Opto-β cells) or electric fields (electrostimulation of Electro-β cells). B) Closed-loop blood-glucose homeostasis. The power circuit of the metabolic fuel cell constantly monitors the blood-glucose levels and switches on the metabolic fuel cell when blood-glucose levels are above 10 mM. The metabolic fuel cell not only reduces the blood-glucose by glucose consumption but also uses the harnessed energy for electro- or opto-stimulation of rapid vesicular insulin release by engineered human cells. The combination of these actions reduces the blood-glucose to normal levels and the metabolic fuel cell is shut off. As a consequence, electro- and optostimulation ceases, as does the insulin release, providing time for an insulin refill before the next glucose surge occurs. The metabolic fuel cell and the human designer cells form a closed-loop control circuit that maintains blood-glucose homeostasis in an automatic, seamless, and self-sufficient manner.

(Figure 2A-iii,iv). The π–π interactions between MWCNTs and PEDOT:PSS harness the electrons from the CuO-mediated glucose-to-gluconate conversion and improve the charge transfer across the entire anode toward the cathode without the need for any mediator (Figure 2A-iv). The anode was stable over time and no changes in the morphology of the 3D nanocomposite were observed even after 60 days of continued use, suggesting that material is sufficiently robust when operating in an implantable metabolic fuel cell (Figure 2A-v,vi). The X-ray diffraction peaks match those of standard cuprous oxide (CuO) monoclinic-phase structure (JCPDS Card No. 48–1548) (Figure S1, Supporting Information).

Electrochemical characterization of the anode nanocomposite showed a clear set of redox peaks for CuO-MWCNTs and CuO-MWCNTs-PEDOT:PSS; these peaks were absent in pristine MWCNTs, indicating that the CuO nanoparticles are indeed generating the redox potential (Figure 2B). Additionally, Nyquist impedance plots analyzed by means of a modified Randle's equivalent circuit revealed that CuO was restraining the transfer of electrons to the MWCNTs, since charge transfer resistance (R_{ct}) exclusively increased when the MWCNTs were decorated with the CuO nanoparticles (CuO-MWCNTs) (Figure 2C). This effect was compensated by the conductive filler PEDOT:PSS, which substantially reduced the overall R_{ct} of the anode nanocomposite CuO-MWCNTs-PEDOT:PSS (Figure 2C; Figure S2, Supporting Information). The peak current increased with higher scan rates, and the anode peak (I_{PA}) and cathode peak (I_{PC}) currents were directly proportional to the square root of the scan rate, which indicates that glucose freely diffuses across the entire metabolic fuel cell (Figure 2D, E).

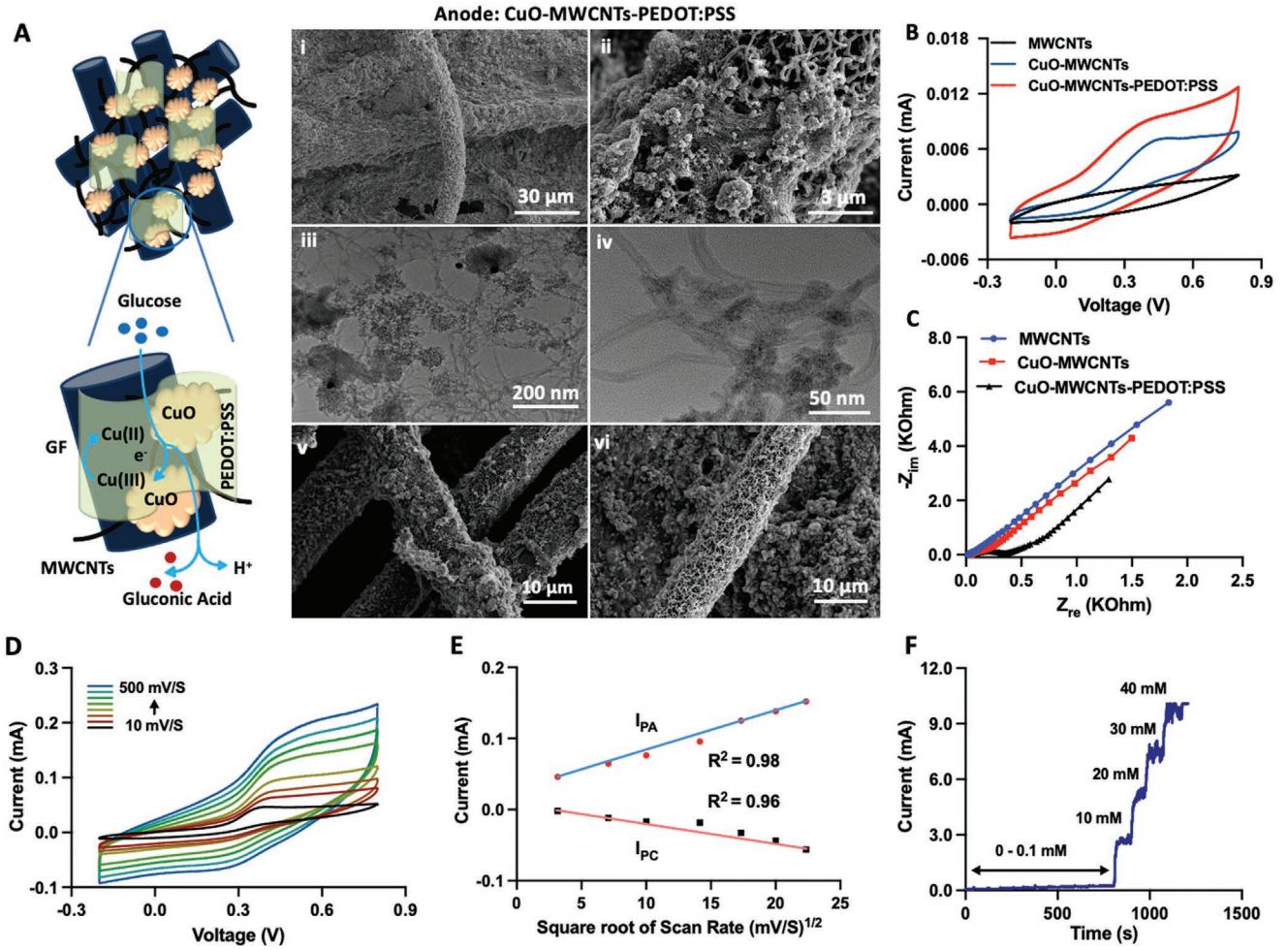

Figure 2. Anode of the non-enzymatic metabolic fuel cell. A) Schematic of the nanocomposite anode material consisting of cupric oxide (CuO) nanoparticles, multi-walled carbon nanotubes (MWCNTs), and poly(3,4-ethylenedioxythiophene)-poly(styrenesulfonate) (PEDOT:PSS) immobilized on a graphite felt (GF). The redox transition of copper catalyzes the conversion of glucose to gluconic acid and a proton (H^+) while releasing a single electron (e^-). i,ii) Field emission scanning electron (FESEM) and iii,iv) transmission electron (TEM) micrographs of CuO/MWCNTs/PEDOT:PSS/graphite felt-modified anode material after v) 1 day and vi) 60 days (FESEM only). B) Cyclic voltammetry and C) impedance spectroscopy of MWCNTs, CuO/MWCNTs, and CuO/MWCNTs/PEDOT:PSS electrodes. Cyclic voltammetry of the CuO/MWCNTs/PEDOT:PSS anodes with different scan rates (10, 50, 100, 200, 300, 400, 500 mV s^{-1}) in presence of D) 10 mM glucose and E) the corresponding correlation between current and scan rates. F) Steady-state amperometric profiling of CuO/MWCNTs/PEDOT:PSS catalytic glucose oxidation at 0.50 V with sequential addition of glucose.

Amperometric glucose sensing confirmed that the anode nanocomposite is highly sensitive to glucose and is fully operational within the human physiological blood-glucose range between 5 mM and 50 mM (Figure 2F; Figure S3, Supporting Information).

2.4. Characterization and Validation of the Cathode

The cathode of the metabolic fuel cells was fabricated by chemical deposition of PtNP on a carbon-black (CB) surface, followed by uniform coating with Nafion (Figure 3A). Nafion coating of the PtNP-CB electrode enables exclusive transfer of protons to the cathode, where they react with PtNP in the presence oxygen to form H_2O. In addition, Nafion efficiently protects the electrode from fouling, which enables continuous use, increases the longevity, and renders the metabolic fuel cell biocompatible for implantation. Conventional platinum cathodes used for classical enzyme-based biofuel cells oxidize in the presence of OH^- radicals leading to Ostwald ripening and fouling of the electrode, which drastically reduce the lifetime and prevent continuous operation in an implant.[40]

Morphological analysis of the cathode by field emission scanning microscopy (FESEM) and transmission electron microscopy (TEM) confirmed the 3D structure of the cathode nanocomposite (Figure 3A), in particular the distinct and uniform decoration of PtNP (Figure 3A-i,ii) (≈2–5 nm in diameter) on the CB surface (≈100 nm in width) as well as the uniform Nafion surface and PtNP-CB intersection coatings (Figure 3A-iii,iv). The cathode was stable for at least 60 days with no apparent morphological change of the 3D nanocomposite, indicating that material is sufficiently robust for operation in an implantable metabolic fuel cell (Figure 3A-v,vi). Importantly, Nafion increases the cohesive force between PtNP and CB as well as

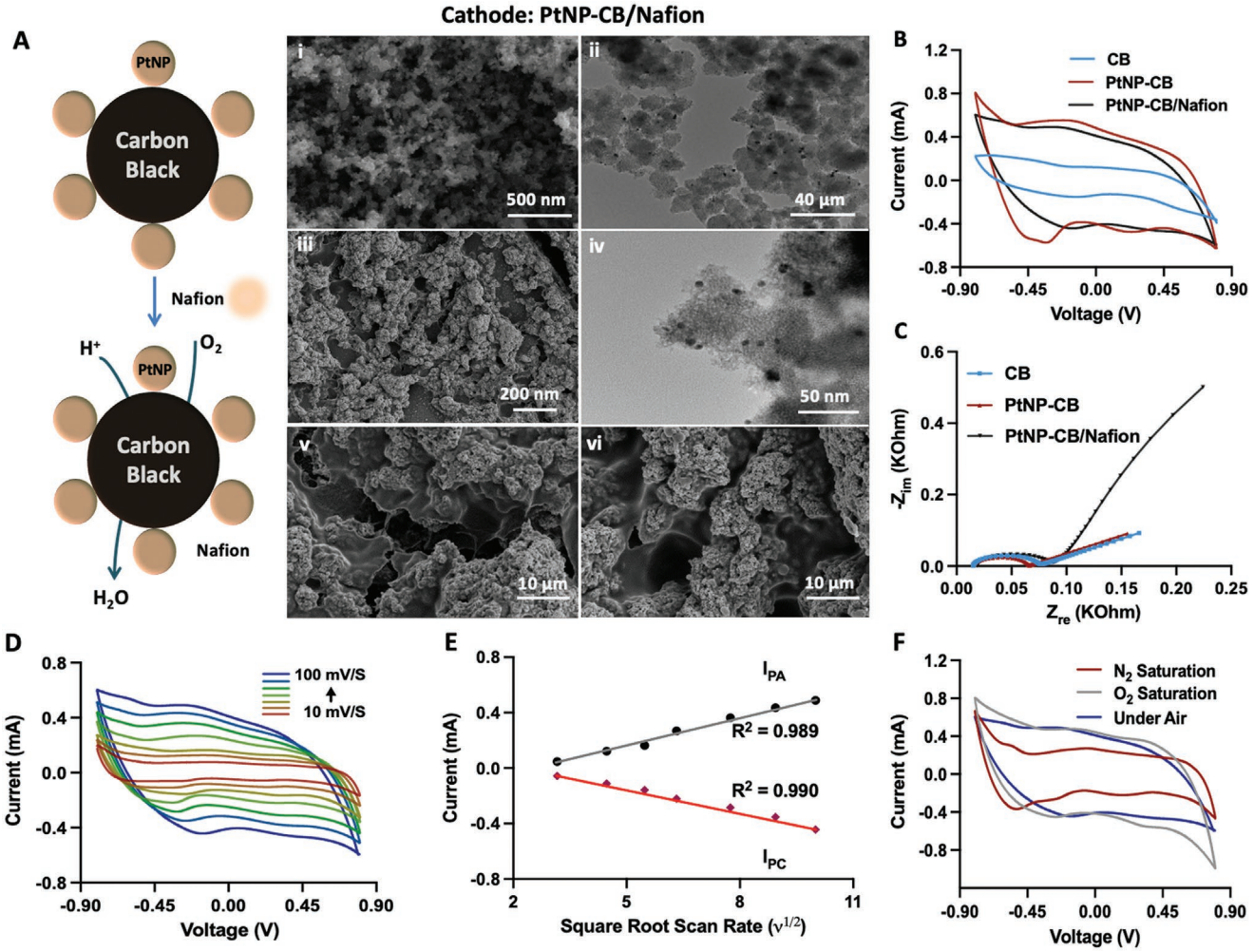

Figure 3. Cathode of the non-enzymatic metabolic fuel cell. A) Schematic of the nanocomposite cathode material consisting of Nafion-coated carbon black (CB)-containing platinum nanoparticles (PtNP). The PtNPs catalyze the reduction of protons (H^+) and oxygen (O_2) to water (H_2O). i,ii) Field emission scanning electron (FESEM) and iii,iv) transmission electron (TEM) micrographs of Nafion-coated platinum nanoparticle-coated carbon black-modified cathode material (PtNP-CB/Nafion) after v) 1 day and vi) 60 days (FESEM only). B) Cyclic voltammetry and C) impedance spectroscopy of carbon black (CB), PtNP-CB, and Nafion-coated PtNP-CB-modified electrodes. Cyclic voltammetry of the Nafion-coated PtNP-CB cathodes with D) different scan rates (10, 20, 30, 40, 60, 80, and 100 mV s^{-1}) and E) the correlation between current and scan rates. F) Cyclic voltammetry of Nafion-coated PtNP-CB cathodes saturated with air, nitrogen cover gas (N_2), and oxygen (O_2) in phosphate-buffered saline (PBS).

improving the longevity of the cathode by boosting the onset potential for oxygen reduction, thereby protecting metabolic fuel cell from biofouling in body fluids.

Cyclic voltammetry (CV) of the cathode revealed that Nafion reduced the electron transfer rate, and that PtNP decoration of the PtNP-CB nanocomposite compensated for this effect (Figure 3B). Likewise, impedance measurements confirmed that the PtNP compensated for the charge transfer resistance (R_{ct}) decrease produced by the Nafion layer (Figure 3C; Figure S2, Supporting Information). Nafion not only serves as the proton-selective membrane of the cathode, it also substantially increases the overall performance, shelf-life, and longevity of the metabolic fuel cell (Figure 3A-v,vi). Cyclic voltammetry (CV) measurements confirmed that the cathode peak (I_{PC}) and anode peak (I_{PA}) currents were linearly related to the square root of the scan rate (Figure 3D), which indicates free diffusion of glucose across the entire metabolic fuel cell (Figure 3E). Cyclic voltammetry (CV) also confirmed the cathode's capacity to efficiently transfer electrons for conversion of protons and oxygen into H_2O (Figure 3F).

2.5. Performance of the Metabolic Fuel Cell

Assembly of the anode and cathode provided a metabolic fuel cell that could be plugged into the mammalian energy system to efficiently generate electrical energy within the physiological blood-glucose range of 4–50 mM (**Figure 4**A–D). Indeed, the basic metabolic fuel cell showed increasing PD and open circuit voltage (OCV) with increasing blood-glucose levels (Figure 4A–D), matching or exceeding the performance of conventional non-physiological biofuel cells that, critically, are neither biocompatible nor implantable. Likewise, the total current density (CD, mA cm^{-2}) also substantially increased

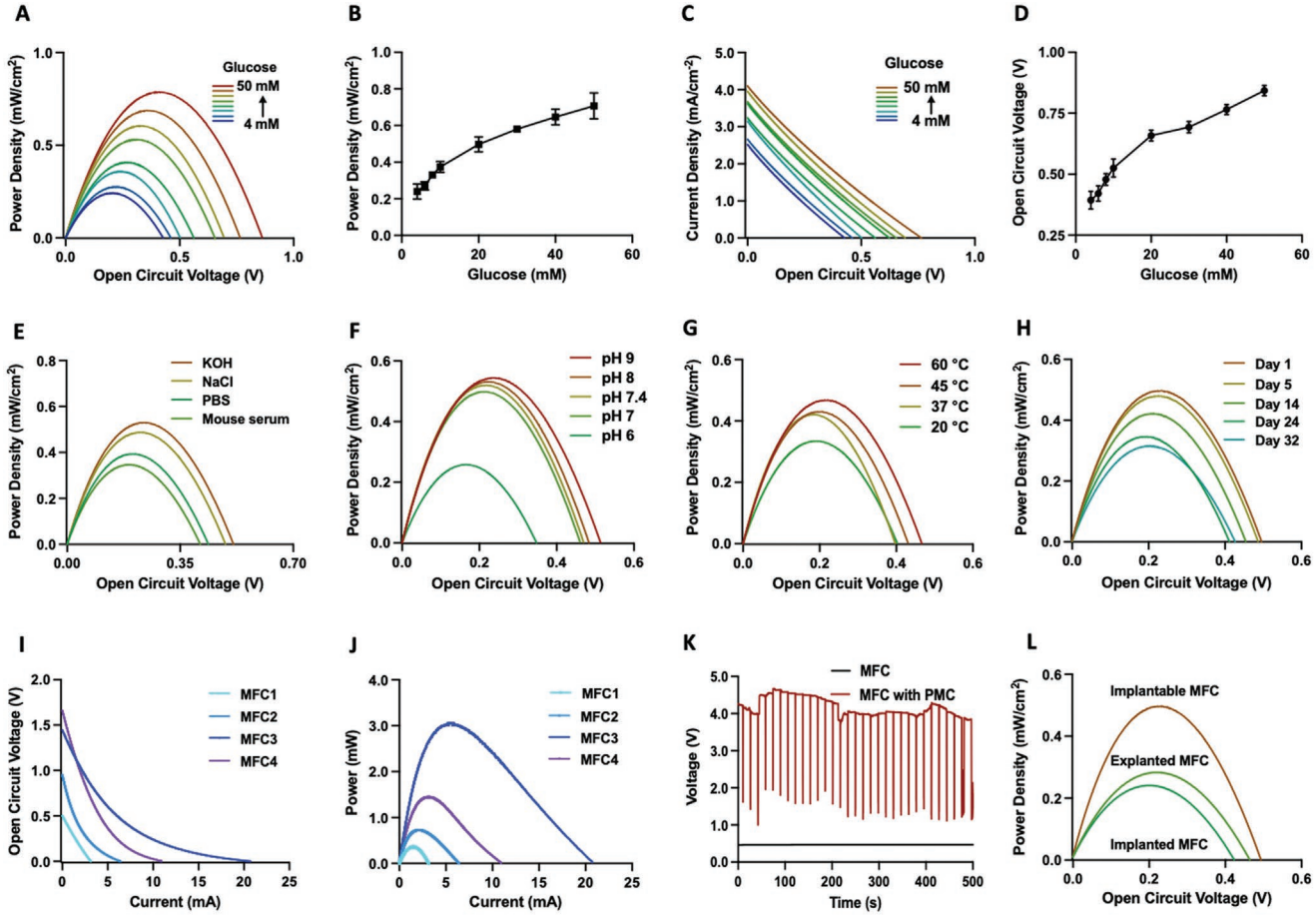

Figure 4. Characterization and performance analysis of the metabolic fuel cell (MFC). A) Power density, B) glucose-dependent power density, C) polarization curves (4, 6, 8, 10, 20, 30, 40, 50 mM glucose), and D) open circuit voltage for different glucose concentrations. Power density of MFCs recorded in the presence of 10 mM glucose under different conditions: E) N_2-purged solutions (PBS, mouse serum, NaCl, and KOH; 0.1 M, 37 °C), F) N_2-purged 0.1 M PBS at different pH values (pH 9.8, 7.4, 7, 6; 37 °C), G) N_2-purged KOH at different temperatures (20 °C, 30 °C, 40 °C, 50 °C; 0.1 M, 37 °C), and H) for different periods of time (1, 5, 14, 24, 32 days, 0.1 M KOH, 37 °C). I) Linear sweep voltammetry polarization and J) power curve for different parallel- and in-series-connected MFCs (MFC1 = 1 in-series MFC, MFC2 = 2 in-series MFCs, MFC 3 = 4 in-series and 2 in-parallel MFCs, MFC 4 = 4 in-series MFCs). K) Open circuit voltage profiling of a single MFC with a power-management circuit (PMC). L) Power densities of a single implantable MFC in vitro, an implanted MFC in a mouse and an MFC explanted after seven days.

under hyperglycemic conditions (Figure 4C). Thus, in principle, the metabolic fuel cell should be able to generate sufficient electrical energy (0.45 mW cm^{-2} (PD), 0.6 V (OCV), or 3.6 mA cm^{-2} (CD)) from blood glucose (10 mM) to power pacemakers (≈10–20 μW),[44] or to light up LEDs for optogenetics (≈4.6 μW).[45]

Besides utilizing blood-glucose in the physiological concentration range as a metabolic energy source, an implanted metabolic fuel cell has to operate in a complex tissue environment with strictly controlled physical (body temperature of 37 °C) and chemical parameters (ionic conductivity of body fluids such as serum, pH of 7.4). Indeed, we found that the metabolic fuel cell generated sufficient energy at 10 mM glucose (Figure 4E–H) in ionic body fluids (Figure 4E), and at physiological pH (Figure 4F) and temperature (Figure 4G), to boot-start a low-power booster while amplifying the output . The performance, stability, and robustness of the metabolic fuel cell were profiled for over a month of continuous use under physiological conditions (10 mM glucose, 37 °C, pH 7.4) (Figure 4H) during time which the device maintained up to 70% of its initial performance. Furthermore, the performance could be restored to 93% simply by washing and heating the device, thereby indicating that it would be reusable (Figure S4, Supporting Information). Considering that real-world biomedical applications would require intermittent operation rather than continuous use, the practical longevity can be expected to be even greater.

2.6. Voltage Management of Metabolic Fuel Cells

To maximize programmable power output for various applications, the metabolic fuel cells can either be stacked in series and/or in parallel or equipped with a power management circuit containing a low-power booster linked to a capacitor (Table S1, Supporting Information),[46,47].We therefore connected basic metabolic fuel cells in different configurations (two or four in series, two in series, and two in parallel) and profiled the OCV as well as total CD in the presence of 10 mM glucose

(Figure 4I,J). While the four-in-series configuration generated the highest OCV (1.65 V; Figure 4I; Table S1, Supporting Information) and continuously maintained 95% of this value for more than 30 h (Figure S5, Supporting Information), the four-in-series arranged in a two set-in-parallel configuration provided the highest total CD (20.71 mA cm^{-2}, Figure 4J; Table S1, Supporting Information). The performance parameters of all the tested metabolic fuel cell configurations compare favorably with those of reported non-enzymatic glucose biofuel cells, and appear to be well suited for powering of bioelectronic devices (Table S1, Supporting Information). However, since implants combining multiple-stacked metabolic fuel cells are too big for real-world clinical applications, we connected a single metabolic fuel cell to a power-management circuit consisting of a low-power boost charger collecting glucose-generated electrical power exclusively during hyperglycemia and charging a capacitor (330 µF) providing a peak voltage of over 4 volts (Figure 4K; Figure S6, Supporting Information).

2.7. In Vivo Characterization of Implanted Metabolic Fuel Cells

To validate the basic metabolic fuel cell in vivo, we implanted the device in type-1-diabetic mice and profiled the resulting OCV (0.42 V) (Figure 4L). While the metabolic fuel cell generated only half of its in vitro PD when implanted, the OCV decreased by only 15% (Figure 4L). The performance decrease of implanted metabolic fuel cells may be associated with the lower ionic conductivity in the tissue as well as possible interference due to fibrosis. However, the overall PD of 0.241 mW cm^{-2} is the highest reported to date for an implanted non-enzymatic metabolic fuel cell. When explanted and refurbished by washing, the performance of the metabolic fuel cells increased to over 100% of that in in vivo operation, which highlights the stability, robustness, and longevity of the device (Figure 4L). To prepare the metabolic fuel cell for therapeutic in vivo applications and to improve its biocompatibility, we deep-coated it with FDA-licensed alginate. This did not significantly alter its key performance values (Figure S7, Supporting Information).

2.8. Closed-Loop Control of Experimental Type-1 Diabetes by the Implanted Metabolic Fuel Cell Stimulating Electrical-Field-Induced Rapid Insulin Secretion

We have recently established that human cells engineered for ectopic co-expression of the L-type voltage-gated channel $Ca_V1.2$ and the inwardly rectifying potassium channel $K_{ir}2.1$ in human cells ($_{Electro}\beta$) rapidly release insulin in response to electrical field-stimulated membrane depolarization.[7] To validate autonomous control of electrical-field-stimulated insulin release by the blood glucose-powered metabolic fuel cell for closed-loop glycemic control, we implanted the metabolic fuel cell connected to $_{Electro}\beta$ cells into type-1-diabetic mice (**Figure 5**A,B).

The metabolic fuel cell was able to generate 4.2 V, which stimulated rapid vesicular secretion of insulin within minutes (Figure 5C). Since glycemic control requires repeated shots of insulin whenever blood-glucose levels are increasing, the metabolic fuel cell needs to repeatedly provide stimulating electrical fields at appropriate intervals. The metabolic fuel cell was indeed able to power repeated hyperglycemia-triggered stimulations of insulin secretion with similar release kinetics and final insulin doses, confirming that the device recharges its power and the $_{Electro}\beta$ cells refill their insulin storage vesicles on an appropriate timescale to program therapeutic insulin doses (Figure 5D). This synchronous reversibility of the implanted metabolic fuel cell and the $_{Electro}\beta$ cells is a prerequisite to establish closed-loop control for the treatment of type-1 diabetes (Figure 5D).

Implantation of the metabolic fuel cell connected to subcutaneous microencapsulated $_{Electro}\beta$ cells into type-1-diabetic mice indeed established closed-loop blood-glucose control integrating hyperglycemia-driven glucose-based electrical energy production by the metabolic fuel cell with electrical field-stimulated rapid vesicular insulin secretion to maintain real-time blood-glucose homeostasis (Figure 5E–H). In type-1-diabetic mice, blood insulin peaked within only 30 min (Figure 5E), restoring blood glucose to wild-type levels without overshoot to hypoglycemia (Figure 5F). Stable wild-type insulin (Figure 5G) and blood-glucose (Figure 5H) levels were maintained during repeated daily feeding over longer periods of time. It is important to note that the power-management circuit of the metabolic fuel cell only releases the voltage to stimulate $_{Electro}\beta$ above a threshold potential of 330 mV reached at a blood-glucose level above 10 mM. The metabolic fuel cell stops catalyzing glucose-based electrical power generation as soon as normoglycemia (<10 mM glucose) is reached, thereby preventing hypoglycemia (Figure 5H). Once the glucose concentration rises above 10 mM, the glucose biofuel cell generates an output voltage above 330 mV, which activates the power-management circuit (PMC) and delivers an output voltage of 4.2 V. As soon as it drops below 10 mM, the PMC is deactivated/switched off to stop the stimulation process.

2.9. Closed-Loop Control Treatment of Experimental Type-1 Diabetes by the Implanted Metabolic Fuel Cell Stimulating Light-Induced Rapid Insulin Secretion

Most bioelectronic implants designed for biomedical applications, in particular those based on optogenetics, will require more power than is needed for electric field stimulation of $_{Electro}\beta$ cells.[6,18,25,48] To validate the metabolic fuel cell for optogenetics, we used it to power blue-light illumination of iβ cells, which are human pancreatic beta cells engineered for blue-light-stimulated vesicular secretion of insulin triggered by the retinal G-protein coupled receptor (GPCR) melanopsin (**Figure 6**A).[17] The implanted metabolic fuel cell was employed to switch on a blue-light-emitting LED during hyperglycemia; the LED illuminates subcutaneous microencapsulated iβ cells to coordinate rapid vesicular insulin release in a closed-loop manner (Figure 6B). The 4.2 volts generated by the metabolic fuel cell was indeed able to power the LED and trigger rapid (within minutes; Figure 6C) and repeated (Figure 6D) vesicular insulin release from iβ cells.

Next, we implanted the metabolic fuel cell connected to microencapsulated iβ cells in type-1-diabetic mice in order to

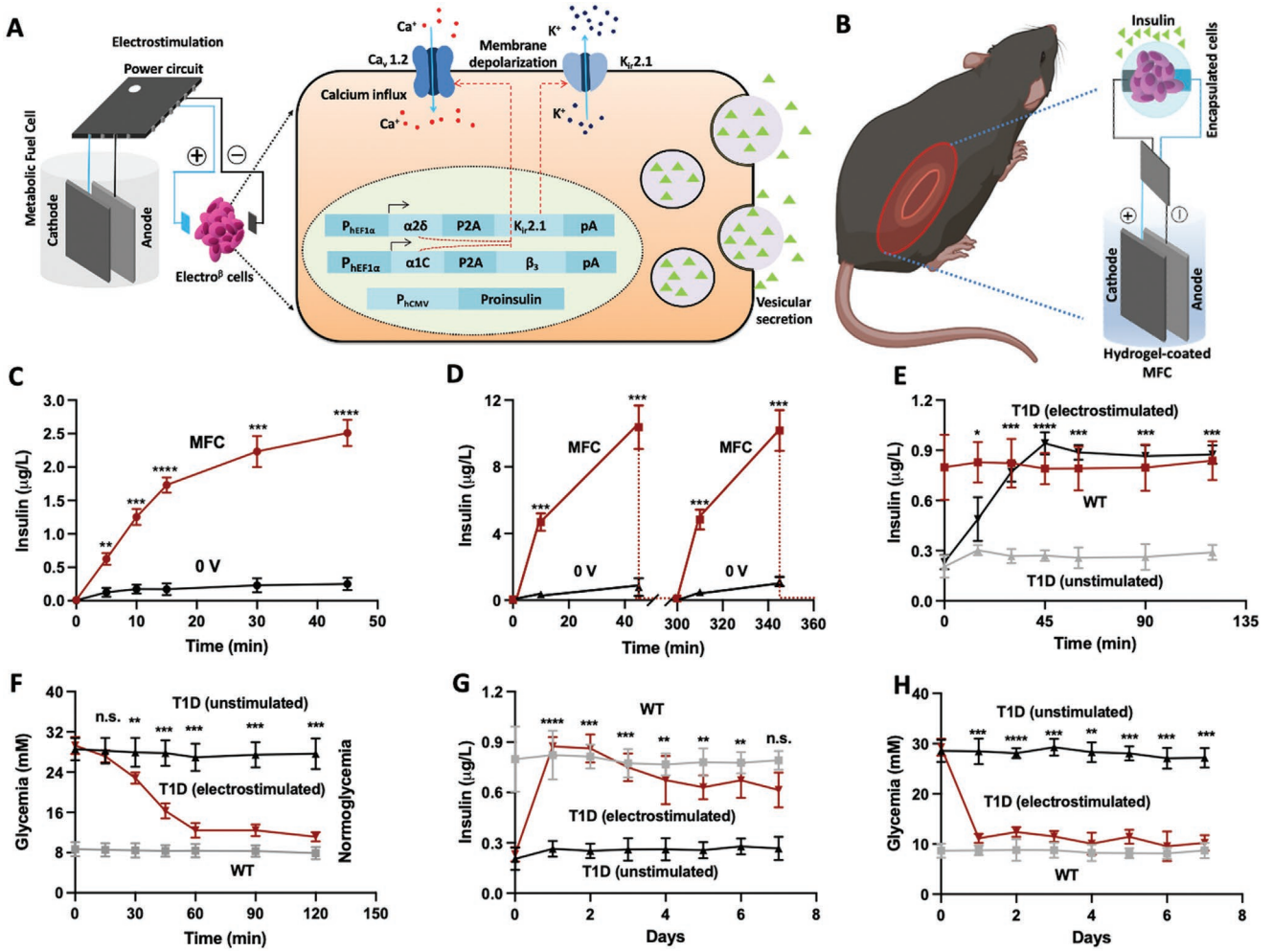

Figure 5. Metabolic fuel-cell-powered electrical field-stimulated vesicular insulin release by engineered human $_{Electro}\beta$ cells. A) Schematic representation of metabolic fuel cell (MFC)-powered insulin secretion by $_{Electro}\beta$ cells. The power management circuit of the metabolic fuel cell controls the conversion of blood glucose into electrical energy and provides the electrical field for the stimulation of the rapid vesicular insulin release by $_{Electro}\beta$ cells. $_{Electro}\beta$ are pancreatic β-cells engineered for constitutive expression of the L-type voltage-gated calcium channel ($Ca_v1.2$) and the inwardly rectifying potassium channel ($K_{ir}2.1$) as well as proinsulin to enable exclusive insulin release in response to electrical field-mediated depolarization. B) Encapsulated $_{Electro}\beta$ cells implanted on the dorsal side were electro-stimulated by a metabolic fuel cell subcutaneously implanted at the dorso-ventral side of a mouse. C) Rapid vesicular insulin secretion by MFC-powered electrical field stimulation of $_{Electro}\beta$ cells (MFC) compared to unstimulated $_{Electro}\beta$ cells (0 V). D) Reversibility of MFC-powered insulin release by $_{Electro}\beta$ cells electro-stimulated twice for 30 min within 5 h. E) Blood-insulin levels and F) corresponding blood-glucose levels of wild-type mice compared to type-1-diabetic mice implanted with MFC-stimulated and unstimulated $_{Electro}\beta$ cells. G) Long-term blood-insulin and H) blood-glucose homeostasis of wild-type mice compared to type-1-diabetic mice implanted with MFC-stimulated and unstimulated $_{Electro}\beta$ cells. Bars represent mean ± SEM, (n = 5). Statistical significance was calculated between stimulated and unstimulated TD1 mice by two-way ANOVA. *$p < 0.05$, **$p < 0.01$, ***$p < 0.001$, ****$p < 0.0001$.

establish closed-loop blood-glucose control. Hyperglycemia-driven glucose-based electrical energy generation by the metabolic fuel cell was successfully integrated with blue-light-stimulated rapid vesicular insulin secretion to maintain blood-glucose homeostasis in real time (Figure 6F–H). In the type-1-diabetic mice, blood insulin peaked within only 30 min (Figure 6E) restoring blood glucose to wild-type levels (Figure 6F). Stable wild-type insulin (Figure 6G) and blood-glucose (Figure 6H) levels were maintained during repeated daily feeding over longer periods of time. Blue-light illumination is only switched on when the metabolic fuel cell is powered at blood-glucose levels above 10 mM glucose, corresponding to a threshold voltage of 330 mV, preventing hypoglycemia (Figure 6H).

3. Conclusion

Wearable and implantable electronic devices have become increasingly powerful for in situ monitoring of physiological information and providing information for real-time medical interventions.[36,49–51] The recent development of biomolecular sensors and designer cells processing and transmitting physiological information to electronic devices as well as electronic devices programming cellular release of biopharmaceuticals in response to light,[17] or direct electrical fields,[7,21,52] has led to the establishment of electro–genetic interfaces that enable reversible communication between biology and electronics,[36,53] sparking visions of novel treatments based on

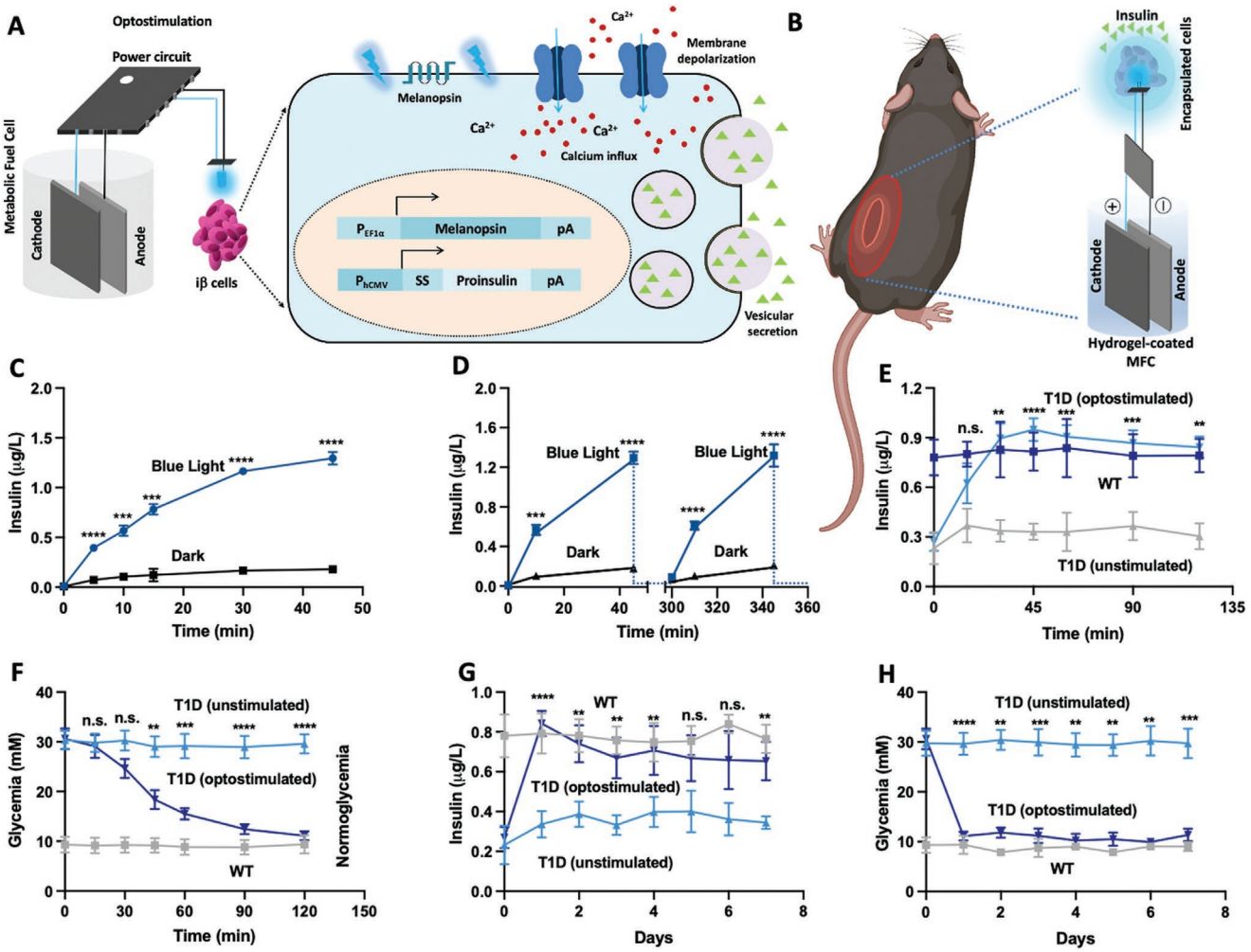

Figure 6. Metabolic fuel-cell-powered optogenetic stimulation of vesicular insulin release by engineered human iβ-cells. A) Schematic representation of metabolic fuel cell (MFC)-powered blue-light-stimulated insulin secretion by iβ-cells. The power management circuit of the metabolic fuel cell controls the conversion of blood glucose into electrical energy and provides the electrical power for blue-light-stimulated optogenetic rapid vesicular insulin release by iβ-cells. iβ-cells are pancreatic β-cells engineered for constitutive expression of melanopsin as well as proinsulin to enable exclusive insulin release in response to blue-light illumination. B) Encapsulated iβ cells implanted on the dorsal side were illuminated by a blue-light LED powered by a metabolic fuel cell subcutaneously implanted at the dorso-ventral side of a mouse. C) Rapid vesicular insulin secretion by MFC-powered blue-light optogenetic stimulation of iβ-cells (blue light) compared to unstimulated iβ-cells (dark). D) Reversibility of MFC-powered insulin release by iβ-cells opto-stimulated twice for 30 min within 5 h. E) Blood-insulin levels and F) corresponding blood-glucose levels of wild-type mice compared to type-1-diabetic mice implanted with MFC-stimulated and unstimulated iβ-cells. G) Long-term blood-insulin and H) blood-glucose homeostasis of wild-type mice compared to type-1-diabetic mice implanted with MFC-stimulated and unstimulated $_{\text{Electro}}\beta$ cells. Bars represent mean ± SEM ($n = 5$). Statistical significance was calculated between stimulated and unstimulated TD1 mice by two-way ANOVA. *$p < 0.05$, **$p < 0.01$, ***$p < 0.001$, ****$p < 0.0001$.

bioelectronic implants.[54,55] No matter whether such bioelectronic devices and implants use light as the middle-man for electro-genetic control,[7,17,18] or direct electro-genetic interfaces based on electrical fields,[21] they all require substantial electrical energy to support monitoring, processing, and communication.[32] Therefore, currently available bioelectronic implants cannot be operated on battery power, but require wired,[18] or wireless power,[6,7] for continuous operation, which limits self-sufficiency, reliability, and patient convenience. Ideally, it would be preferable to operate bioelectronic implants using an endogenous power source for self-sufficient, continuous, and reliable operation. In principle, body fluids contain sufficient excess metabolic energy in the form of fatty acids,[56] and glucose,[57] which could be harnessed to power bioelectronic implants as well as wearable electronic devices. Since fatty acid metabolism is functionally linked with glucose production via gluconeogenesis.[58,59] and glucose levels often increase and spike due to dietary habits and lifestyle in industrializing countries, or are chronically increased in diabetes, which affects over 10% of the global population,[60,61] excess blood sugar could be an optimal metabolic energy source to power bioelectronic implants.

An ideal glucose-powered metabolic fuel cell should produce high levels of electrical energy during hyperglycemic conditions, where blood glucose concentration exceeds 10 mM. First-generation glucose biofuel cells required glucose oxidase for catalytic breakdown of glucose into gluconate to generate

electrons as a source of electrical power.[30,62] Although enzyme-based glucose biofuel cells have seen impressive improvements over the past decade, boosting power-generation efficiency to oOCV of almost 800 mV, the limited shelf-life of the enzymes and the need for glucose concentrations two orders of magnitude above physiological blood-sugar levels have prevented any biomedical applications. Typical results include: >300 mM glucose, 298 mV;[63] >300 mM glucose, 370 mV;[40] 1 M glucose, 750 mV;[64] 200 mM glucose, 360 mV;[65] 170 mM glucose, 770 mV.[66]

Second-generation glucose biofuel cells replaced glucose oxidase with metal–organic frameworks (MOFs) containing mesoporous $CuCo_2O_4$ (100 mM glucose, 850 mV),[67] carbon nanotubes decorated with Co_3O_4 nanododecahedras (100 mM glucose, 298 mV),[68] graphene nanosheets decorated with nickel oxide (100 mM glucose, 750 mW),[69] or cerium oxide ceramics (500 mM glucose, 110 mV).[70] Although the replacement of glucose oxidase by metal oxides was an important step in increasing the stability and longevity of glucose biofuel cells, their need for glucose levels orders of magnitude beyond the physiological range and their non-flexible rigid structure render them incompatible with bioelectronic implants and biomedical applications. The performance parameters of recently developed enzymatic and non-enzymatic glucose biofuel cells are compared in Table S2, Supporting Information.

Here, by integrating a hierarchically-decorated flexible 3D nanostructured inorganic CuO catalyst, we fabricated a metabolic fuel cell generating an OCV of over 330 mV at physiological blood-glucose concentrations. The efficient conversion of metabolic to electrical energy is mediated by nanocatalytic CuO, which converts glucose into gluconate and generates protons, while transferring the resulting electrons by ballistic transport through the backbone of MWCNTs coherently supported by the conductive filler PEDOT:PSS. This filler interacts with free π electrons on the walls of the MWCNTs, leading to π–π conjugation wherein PEDOT oligos form conductive clusters aligned to the PSS chains, thereby forming localized conducting grains which increase the ballistic transport of electrons. The resulting metabolic fuel cell not only efficiently sensed glucose across the entire physiological blood-glucose range, but also maintained its performance and stability over extended periods of time. The harnessing of electrons by the catalytic breakdown of glucose at the anode was combined with a smart, mediator-free nanocomposite Nafion-coated cathode, where incoming protons serve to reduce oxygen to H_2O. The 3D architecture of the metabolic fuel cell increases the reaction area and maximizes the electron entrapment efficiency and transport capacity.

While today's drug-based medications are open-loop control systems for which physicians generally prescribe a number of pills to be taken several times a day based on the patient's body weight,[71,72] most metabolic activities are maintained at homeostatic levels by closed-loop circuits in which the output feedback-controls the input. For example, blood-glucose homeostasis is mainly controlled by pancreatic beta cells which constantly monitor blood sugar.[73] The beta cells detect postprandial blood-glucose surges and release insulinogenic peptide hormones such as insulin, which promotes cellular glucose uptake and restores blood-glucose homeostasis. Including a power-management circuit in the metabolic fuel cell not only boosted the OCV to levels able to power bioelectronic devices, such as rapid vesicular insulin release by direct electrical field-stimulated $_{Electro}\beta$ cells (1 V) or blue-light-stimulated iβ cells (3 V), but also enabled the fuel cell to drive electro- or opto-stimulated insulin release by implanted designer cells exclusively under hyperglycemic conditions, when the OCV rose above 330 mV. Thus, the metabolic fuel cell behaves like a human beta cell, constantly monitoring blood-glucose levels and stimulating rapid cellular release of insulin during hyperglycemia to restore blood-glucose homeostasis. The fact that the metabolic fuel cell achieves the glucose-lowering effect by a combination of stimulating insulin release and consuming glucose for electrical power production enables glucose homeostasis to be maintained at lower insulin levels, which would be therapeutically relevant, particularly in cases of insulin resistance.[74,75]

In this work, we have validated our fully integrated, implantable, non-enzymic glucose metabolic fuel cell for closed-loop electro- and opto-genetic control of insulin delivery, and confirmed that it can restore and maintain glucose homeostasis in experimental type-1 diabetes. The availability of metabolic fuel cells converting excess metabolic energy into electrical power under physiological conditions can be expected to open up many new opportunities for application of bioelectronic implants as well as wearable electronic devices.

4. Experimental Section

Reagents and Materials for the Metabolic Fuel Cell and Power Circuit Fabrication and Characterization: Acrylic acid ($C_3H_4O_2$), chloroplatinic acid (H_2PtCl_6), copper chloride dihydrate ($CuCl_2{\cdot}H_2O$), glucose, hydroxylamine hydrochloride ($NH_2OH{\cdot}HCl$), Nafion 117 solution (cat. no. 70160, $C_7HF_{13}O_5S{\cdot}C_2F_4$), *N*-hydroxysuccinimide (NHS, $C_4H_5NO_3$), phosphate-buffered saline (PBS, cat. no. P5493), *N*,*N*′-bis(acryloyl) cystamine (BAC, $C_{10}H_{16}N_2O_2S_2$), polycellulose ($[C_{12}H_{20}O_{10}]_n$), sodium borohydride ($NaBH_4$), sodium dodecyl sulfate (SDS, $NaC_{12}H_{25}SO_4$), 1-ethyl-3-(-3-dimethylaminopropyl)carbodiimide (EDC, $C_8H_{17}N_3$), 2,2′-azobis(2-methylpropionamidine) dihydrochloride (AAPH, $C_8H_{20}Cl_2N_6$), and PEDOT:PSS were purchased from Sigma-Aldrich. Acetone, CB, ethanol, potassium hydroxide (KOH), and sodium hydroxide (NaOH) were purchased from ThermoFisher Scientific. MWCNTs functionalized with —COOH groups were purchased from Nanocyl Inc. (cat. no. 7000). All reagents were used as received without further purification. Insulating copper wire and silver ink (cat. no. 186–3600) were purchased from RS Components. Graphite felt (GF) (cat. no. G100) was purchased from Fuel Cell Store. Bio glue (cat. no: BG3510-5-US) was purchased from CryoLife Inc. The low-power boost charger BQ25504 (Texas Instruments) was purchased from Digi-Key Inc. and the 330 µF capacitor (Panasonic, tantalum capacitor; cat. no. 10TPB330M) from Distrelec.

Fabrication of the Metabolic Fuel Cell Anode Design: CuO was prepared by mixing 1.5 g of sodium dodecyl sulfate (SDS) with 200 mL ddH_2O while stirring (1 h, 200 rpm, 50 °C), followed by sequential addition of 100 mL of a 1:1 v/v mixture of 0.2 M $CuCl_2{\cdot}H_2O$ and 0.5 M KOH as well as of 10 mL of 0.2 M hydroxylamine hydrochloride while stirring for another 4 h at 200 rpm and 140 °C. The CuO precipitate was washed five times with ddH_2O by centrifugation for 5 min at 8000 × *g* and dried overnight at 180 °C.[76] Subsequently, 100 mg CuO and 10 mg of MWCNTs were added to 10 mL PEDOT:PSS solution (10% v/v dissolved in DMSO by bath sonication (Bioruptor, Diagenode), stirred (30 min, 200 rpm, 30 °C), and probe-sonicated for 10 min (82% amplitude, 20 kHz, 250 W, 5 s on/off cycles; Sonopuls HD4100, Bandelin Electronic GmbH) to produce a homogenous CuO-MWCNTs-PEDOT:PSS solution. To produce the anode, 1 cm^2 GF (washed 5× in 75% ethanol, rinsed 5× in

ddH_2O, dried at 60 °C overnight) were dip-coated with CuO-MWCNTs-PEDOT:PSS solution and dried for 2 h at 150 °C four times consecutively to produce a uniform coating.

Cathode Design: PtNP-decorated CB (PtNP-CB) was produced by first dissolving 1 mg mL^{-1} CB powder (CB) in 100 mL 75% ethanol while stirring (30 min, 300 rpm, 40 °C), followed by sequential addition of 50 mL of chloroplatinic acid (1 mg mL^{-1} in ddH_2O) while stirring (4 h, 300 rpm, 80 °C) and dropwise addition of 5 mL of 0.1 M $NaBH_4$ while stirring for 30 min at 300 rpm and 80 °C. The PtNP-CB precipitate was washed five times with ddH_2O by centrifugation for 5 min at 8000 × *g* and dried for 4 h at 120 °C. To produce the cathode, 1 cm^2 CC (washed 5× in propanol, rinsed 5× in ddH_2O, dried overnight at 60 °C) was dip-coated with PtNP-CB solution and dried for 2 h at 60 °C four times consecutively to produce a uniform coating. Nafion 117 solution was then drop-cast onto PtNP-CB-coated CC and the Nafion coating on PtNP-CB was repeated another four times before drying the cathode overnight at 60 °C.

Assembly: Anode and cathode were connected via thin insulated copper wires using silver ink and BioGlue for sealing and protection. Anodes and cathodes were separated and packed into a polycellulose membrane bag that was sealed with BioGlue.

Encapsulation of the Metabolic Fuel Cell: In order to protect and insulate the metabolic fuel cell from the tissue environment it was encapsulated in clinically licensed alginate. The metabolic fuel cell was packed in a cellulose dialysis membrane and further coated in alginate hydrogel, which is a biocompatible FDA-licensed biomaterial used in many proof-of-concept animal studies,[7,17,77–79] as well as in human clinical trials (ClinicalTrials.gov, e.g., NCT01379729, NCT00790257, NCT01739829).[80] The alginate shell was prepared by dissolving 1.6 g of alginate (cat. no. 11061528; Büchi AG) in 100 mL aqueous solution containing 3% w/w acrylic acid, 0.01% w/w *N*,*N*′-bis(acryloyl) cystamine (BAC) and 0.05% w/w 2,2′-azobis(2-methylpropionamidine) dihydrochloride (AAPH), stirring (30 min, 300 rpm, 60 °C), and dropwise addition of 10 mL of an aqueous solution containing 5 mL of 1% w/w 1-ethyl-3-(-3-dimethylaminopropyl)carbodiimide (EDC) and 5 mL of 0.5% w/w *N*-hydroxysuccinimide (NHS). The metabolic fuel cell was deep-coated by immersion first in the resulting alginate solution for 1 h and then for another hour in 0.1 M aqueous calcium chloride solution to gel the alginate. The alginate-coated metabolic fuel cells were stored at 4 °C until implantation.

Power-Management Circuit: A power-management circuit was designed for the metabolic fuel cell to harvest the energy, boost the voltage, and release the power to activate the blue LED or the electrical field at blood-glucose levels above 10 mM. The power-management circuit consisted of a low-power boost charger (BQ25504 Texas Instruments; Digi-Key Inc., cat. no. Q25504RGTT) connected to a 330 µF capacitor (Panasonic, tantalum capacitor; cat. no. 10TPB330M, Diselectric) which was charged by the metabolic fuel cell to obtain a final output voltage of 4.2 V from the low-power boost charger. The circuit diagram of the power management circuit is shown in Figure S6, Supporting Information.

Characterization of the Metabolic Fuel Cell: Anode and cathode morphologies were characterized using field emission scanning electron microscopy (FESEM; FEI Versa 3D Dualbeam, ThermoFisher Scientific) and transmission electron microscopy (TEM; FEI Tecnai G2 Spirit, ThermoFisher Scientific). The crystal structure of the metabolic fuel cell was analyzed using a single-crystal diffractometer (Bruker Kappa Apex II, Bruker corporation, Billerica, MA, USA) set to the Kα radiation of Cu (λ = 1.542 Å). Cyclic voltammetry, polarization curves, electrical impedance spectroscopy, and open circuit potential of the metabolic fuel cell were analyzed in phosphate-buffered saline (PBS; pH 7.4) at 37 °C. The CD, OCV, and PD were calculated based on the anode surface area. For electrochemical measurements, an Ag/AgCl electrode was used as the reference, while a platinum wire was used as the counter electrode. Power was calculated according to the following Equation (1):

$$P = V \times I \tag{1}$$

where *P* is power (W), *V* is voltage (V), and *I* is current (A).

Cultivation and Stimulation of $_{Electro}\beta$ *and i*β *Cells*: $_{Electro}\beta$ cells (electro-sensitive human β-cells),[7] and iβ cells (iPhone-induced insulin release in β-cells),[17] were monoclonal cell lines based on the 1.1.E7,[81] -derived glucose-insensitive pancreatic human cell line INS_{Vesc},[7] engineered for constitutive expression of either i) Cav1.2 and Kir2.1 channels to promote rapid vesicular insulin release in response to electrical fields,[7] or ii) the retinal GPCR melanopsin to trigger rapid vesicular insulin release in response to blue light.[17,18] Both cell lines were cultivated in Roswell Park Memorial Institute 1640 medium (RPMI; cat. no. 72400-021, ThermoFisher Scientific) supplemented with 10% v/v fetal bovine serum (FBS, cat. no. F7524, lot no. 0001638271; Sigma-Aldrich) and optionally 1% v/v penicillin/streptomycin solution (P/S, 100 U mL^{-1} penicillin and 100 µg mL^{-1} streptomycin; cat. no.15140-122, lot no. 147173; ThermoFisher Scientific). For electrostimulation, 1×10^5 $_{Electro}\beta$ cells were seeded per well of a 6-well plate containing 1.4 mL of culture medium and cultivated for 24 h before they were electro-stimulated for the indicated periods of time using a C-Dish cover (IonOptix Inc.). Pairs of carbon electrodes were placed in the culture medium,[7] and connected to the metabolic fuel cell (4.2 V) for stimulation. For optogenetic stimulation, 1.5×10^4 iβ cells were seeded per well of a 96-well plate containing 100 µL of cell culture medium and cultivated for 24 h before they were illuminated for the indicated periods of time using a 96-well plate compatible blue-light LED (475 nm, cat. no. B56L5111P; Roithner Lasertechnik GmbH) array cover,[7] powered by the metabolic fuel cell (4.2 V). Insulin levels were profiled at the indicated time points after stimulation using an ultrasensitive ELISA assay (cat. no. 10-1247-01; Mercordia).

Microencapsulation of $_{Electro}\beta$ *and i*β *Cells*: To protect the human $_{Electro}\beta$ and iβ cells from the mouse immune system while enabling free diffusion of nutrients and therapeutic proteins such as insulin, clinical trial-validated, FDA-licensed alginate-based encapsulation technology was used.[80] Prior to microencapsulation, $_{Electro}\beta$ and iβ cells were grown to 80% confluence in standard cultivation medium (DMEM, 10% FBS), trypsinized and resuspended at 3.5×10^7 cells per mL in 3-(*N*-morpholino)propanesulfonic acid (MOPS) buffer (10 mM MOPS, 0.85 NaCl, pH 7.2). $_{Electro}\beta$ and iβ cells were microencapsulated in coherent alginate-poly(L-lysine) (PLL)-alginate microcapsules (500 cells per capsule) of 400 µm in diameter by mixing 7×10^7 cells with 12 mL alginate (cat. no. 11061528; Büchi AG), 200 mL 0.05% PLL solution (cat. no. PLKB50, Alamanda Polymers). The encapsulator (B-395 Pro, Büchi AG) was set to the following parameters: 200 µm nozzle with a vibration frequency of 1000 Hz, a 25 mL syringe operated at a flow rate of 20 mL min^{-1} and 1.2 kV voltage for bead dispersion. After harvesting, the capsules were resuspended for 10 min in 200 mL 0.05% PLL solution to provide an additional layer of PLL for improved biocompatibility.

Animal Experiments. Experimental Type-1 Diabetes: Type-1 diabetic (T1D) mice were generated by injecting 8-week-old male wild-type C57BL/6JRJ mice (25 g, Janvier Labs) intraperitoneally (IP) on 4 consecutive days with streptozotocin (STZ; 50 mg kg^{-1}, 0.2 M citrate buffer, pH 4.2; cat. no. S0130, Sigma-Aldrich) after fasting for 6 h.[82] Non-diabetic control animals received injections without STZ. After 1 week, the T1D status of the STZ-treatment group was confirmed by quantifying the persistent fasting hyperglycemia using clinically licensed ContourNext test strips and the ContourNext ONE reader (Ascensia Diabetes Care; cat. nos. 84191451 and 85659367, respectively).

Implantation of Microencapsulated Cells and the Metabolic Fuel Cell: The dorsal and dorsoventral sides of the mice were shaved and the animals were anesthetized using 4% isoflurane and maintained under 2% isoflurane during surgical interventions. The microencapsulated cells were subcutaneously implanted by injection (0.5 mL DMEM, 5×10^6 $_{Electro}\beta$ or iβ cells, 500 cells per capsule) on the dorsal side using a standard 5 mL syringe equipped with a 21-gauge needle, which strategically placed the cells in the region just below the cervical vertebrae to minimize aseptic loosening of the microencapsulated cells. After stabilizing the mice for 6 h, the metabolic fuel cell was implanted via surgical incision subcutaneously at the dorsoventral side and connected either via wired platinum electrodes directly to the implanted $_{Electro}\beta$ cells for electrical-field-mediated stimulation or to the blue LED (475 nm, cat. no. B56L5111P, Roithner LaserTechnik GmbH)

to directly illuminate the implanted iβ cells from a distance of 5 mm. Blood glucose was profiled using clinically licensed ContourNext test strips and the ContourNext ONE reader (Ascensia Diabetes Care; cat. nos. 84191451 and 85659367, respectively) and blood-insulin levels were quantified in serum collected in Microtainer serum separator tubes (centrifugation 10 min, 6000 × *g*; cat. no. 365967, Becton Dickinson), using an ultrasensitive ELISA assay (cat. no. 10-1247-01, Mercordia,).

Animal Experimentation Licenses: All animal experiments were approved by the authorities of the Canton of Basel-Stadt, Switzerland (license number: 2996_34477) and conducted by P.G.R. (license number: LTK 5507) at the Department of Biosystems Science and Engineering (D-BSSE) of the ETH Zurich in Basel, Switzerland.

Statistical Analysis: All data sets were analyzed using GraphPad Prism software (version 8.4.3, La Jolla, CA, USA), following a two-way ANOVA *t* test. The criterion for a significant difference between data sets was $p < 0.05$. All experiments data are presented as mean ± standard deviation (SD) for $n = 3$ or $n = 5$, as noted in the figure legends.

Supporting Information

Supporting Information is available from the Wiley Online Library or from the author.

Acknowledgements

The authors thank Marie-Didiée Hussherr for support with animal experimentation and Henryk Zulewski as well as Ana Palma Teixeira for generous advice. This work was financially supported through a European Research Council advanced grant (ElectroGene, no. 785800) and in part by the Swiss National Centre of Competence in Research (NCCR) for Molecular Systems Engineering. D.M., P.G.R., and M.F. designed the project, analyzed the results, and wrote the manuscript. D.M., P.G.R., and M.M. conducted the in vitro experiments. P.G.R. performed the animal experiments. P.B. designed and fabricated the power circuit.

Open access funding provided by Eidgenossische Technische Hochschule Zurich.

Conflict of Interest

The authors declare no conflict of interest.

Data Availability Statement

The data that support the findings of this study are available from the corresponding author upon reasonable request.

Keywords

beta cells, biofuel, glucose, hyperglycemia, metabolic fuel cell, stimulation, type-1 diabetes

Received: January 30, 2023
Revised: February 28, 2023
Published online:

[1] A. J. Bandodkar, P. Gutruf, J. Choi, K. H. Lee, Y. Sekine, J. T. Reeder, W. J. Jeang, A. J. Aranyosi, S. P. Lee, J. B. Model, R. Ghaffari, C. J. Su, J. P. Leshock, T. Ray, A. Verrillo, K. Thomas, V. Krishnamurthi, S. Han, J. Kim, S. Krishnan, T. Hang, J. A. Rogers, *Sci. Adv.* **2019**, *5*, eaav3294.
[2] J. Jang, J. Kim, H. Shin, Y. G. Park, B. J. Joo, H. Seo, J. E. Won, D. W. Kim, C. Y. Lee, H. K. Kim, J. U. Park, *Sci. Adv.* **2021**, *7*, eabf7194.
[3] M. Mansouri, M. D. Hussherr, T. Strittmatter, P. Buchmann, S. Xue, G. Camenisch, M. Fussenegger, *Nat. Commun.* **2021**, *12*, 3388.
[4] C. Shi, Z. Zou, Z. Lei, P. Zhu, W. Zhang, J. Xiao, *Sci. Adv.* **2020**, *6*, eabd0202.
[5] H. Yeon, H. Lee, Y. Kim, D. Lee, Y. Lee, J. S. Lee, J. Shin, C. Choi, J. H. Kang, J. M. Suh, H. Kim, H. S. Kum, J. Lee, D. Kim, K. Ko, B. S. Ma, P. Lin, S. Han, S. Kim, S. H. Bae, T. S. Kim, M. C. Park, Y. C. Joo, E. Kim, J. Han, J. Kim, *Sci. Adv.* **2021**, *7*, eabg8459.
[6] M. Folcher, S. Oesterle, K. Zwicky, T. Thekkottil, J. Heymoz, M. Hohmann, M. Christen, M. D. El-Baba, P. Buchmann, M. Fussenegger, *Nat. Commun.* **2014**, *5*, 5392.
[7] K. Krawczyk, S. Xue, P. Buchmann, G. Charpin-El-Hamri, P. Saxena, M. D. Hussherr, J. Shao, H. Ye, M. Xie, M. Fussenegger, *Science* **2020**, *368*, 993.
[8] J. Rivnay, H. Wang, L. Fenno, K. Deisseroth, G. G. Malliaras, *Sci. Adv.* **2017**, *3*, 1601649.
[9] L. J. Boddington, J. P. Gray, J. M. Schulz, J. N. J. Reynolds, *Exp. Neurol.* **2020**, *323*, 113071.
[10] M. Tigges, T. T. Marquez-Lago, J. Stelling, M. Fussenegger, A. Prindle, P. Samayoa, I. Razinkov, T. Danino, L. S. Tsimring, J. Hasty, *Nature* **2012**, *457*, 309.
[11] M. Tigges, T. T. Marquez-Lago, J. Stelling, M. Fussenegger, *Nature* **2009**, *457*, 309.
[12] A. Prindle, P. Samayoa, I. Razinkov, T. Danino, L. S. Tsimring, J. Hasty, *Nature* **2012**, *481*, 39.
[13] M. Müller, S. Ausländer, A. Spinnler, D. Ausländer, J. Sikorski, M. Folcher, M. Fussenegger, *Nat. Chem. Biol.* **2017**, *13*, 309.
[14] S. Auslände, D. Ausländer, M. Müller, M. Wieland, M. Fussenegger, *Nature* **2012**, *487*, 123.
[15] P. Karagiannis, Y. Fujita, H. Saito, *Proc. Jpn. Acad., Ser. B* **2016**, *92*, 412.
[16] O. Madderson, A. P. Teixeira, M. Fussenegger, *Curr. Opin. Chem. Biol.* **2021**, *64*, 98.
[17] M. Mansouri, S. Xue, M. Hussherr, T. Strittmatter, G. Camenisch, M. Fussenegger, *Small* **2021**, *17*, 2101939.
[18] H. Ye, M. D. El Baba, R. W. Peng, M. Fussenegger, *Science* **2011**, *332*, 1565.
[19] S. A. Stanley, J. Sauer, R. S. Kane, J. S. Dordick, J. M. Friedman, *Nat. Med.* **2015**, *21*, 92.
[20] B. A. Stefanov, A. P. Teixeira, M. Mansouri, A. Bertschi, K. Krawczyk, G. C. El Hamri, S. Xue, M. Fussenegger, *Adv. Sci.* **2021**, *8*, 2101813.
[21] M. Zhao, B. Song, J. Pu, T. Wada, B. Reid, G. Tai, F. Wang, A. Guo, P. Walczysko, Y. Gu, T. Sasaki, A. Suzuki, J. V. Forrester, H. R. Bourne, P. N. Devreotes, C. D. McCaig, J. M. Penninger, *Nature* **2006**, *442*, 457.
[22] X. Ma, Y. Lu, Z. Zhou, Q. Li, X. Chen, W. Wang, Y. Jin, Z. Hu, G. Chen, Q. Deng, W. Shang, H. Wang, H. Fu, X. He, X. H. Feng, S. Zhu, *Sci. Adv.* **2022**, *8*, eabk1826.
[23] C. L. Maikawa, A. I. D'Aquino, R. A. Lal, B. A. Buckingham, E. A. Appel, *Sci. Transl. Med.* **2021**, *13*, eabd6726.
[24] K. G. Maxwell, P. Augsornworawat, L. Velazco-Cruz, M. H. Kim, R. Asada, N. J. Hogrebe, S. Morikawa, F. Urano, J. R. Millman, *Sci. Transl. Med.* **2020**, *12*, eaax9106.
[25] J. Shao, S. Xue, G. Yu, Y. Yu, X. Yang, Y. Bai, S. Zhu, L. Yang, J. Yin, Y. Wang, S. Liao, S. Guo, M. Xie, M. Fussenegger, H. Ye, *Sci. Transl. Med.* **2017**, *9*, eaal2298.
[26] P. Zimmet, K. G. Alberti, D. J. Magliano, P. H. Bennett, *Nat. Rev. Endocrinol.* **2016**, *12*, 616.
[27] K. Torigoe, M. Takahashi, K. Tsuchiya, K. Iwabata, T. Ichihashi, K. Sakaguchi, F. Sugawara, M. Abe, *ACS Omega* **2018**, *3*, 18323.

[28] A. J. Wargacki, E. Leonard, M. N. Win, D. D. Regitsky, C. N. S. Santos, P. B. Kim, S. R. Cooper, R. M. Raisner, A. Herman, A. B. Sivitz, A. Lakshmanaswamy, Y. Kashiyama, D. Baker, Y. Yoshikuni, *Science* **2012**, *335*, 308.
[29] Y. Chen, S. Lu, S. Zhang, Y. Li, Z. Qu, Y. Chen, B. Lu, X. Wang, X. Feng, *Sci. Adv.* **2017**, *3*, e1701629.
[30] D. A. Gough, L. S. Kumosa, T. L. Routh, J. T. Lin, J. Y. Lucisano, *Sci. Transl. Med.* **2010**, *2*, 42ra53.
[31] M. Frei, J. Martin, G. Cristiano, R. Zengerle, S. Kerzenmacher, *J. Power Sources* **2018**, *401*, 403.
[32] D. Lee, S. H. Jeong, S. Yun, S. Kim, J. Sung, J. Seo, S. Son, J. T. Kim, L. Susanti, Y. Jeong, S. Park, K. Seo, S. J. Kim, T. D. Chung, *Biosens. Bioelectron.* **2021**, *171*, 112746.
[33] A. Zebda, C. Gondran, A. L.e Goff, M. Holzinger, P. Cinquin, S. Cosnier, *Nat. Commun.* **2011**, *2*, 370.
[34] Y. Hubenova, M. Mitov, *Bioelectrochemistry* **2015**, *106*, 177.
[35] S. Hao, X. Sun, H. Zhang, J. Zhai, S. Dong, *J. Mater. Chem. B* **2020**, *8*, 3393.
[36] Y. Yu, J. Nassar, C. Xu, J. Min, Y. Yang, A. Dai, R. Doshi, A. Huang, Y. Song, R. Gehlhar, A. D. Ames, W. Gao, *Sci. Rob.* **2020**, *5*, eabh3328.
[37] R. A. S. Luz, A. R. Pereira, J. C. P. de Souza, F. C. P. F. Sales, F. N. Crespilho, *ChemElectroChem* **2014**, *1*, 1751.
[38] I. Jeerapan, J. R. Sempionatto, J. Wang, *Adv. Funct. Mater.* **2020**, *30*, 1906243.
[39] M. Mehak, Y. D. Kumar, S. R. Kishore, S. Gurmeet, *Biofuel Cells* **2021**, *12*, 317.
[40] C. H. Kwon, Y. Ko, D. Shin, M. Kwon, J. Park, W. K. Bae, S. W. Lee, J. Cho, *Nat. Commun.* **2018**, *9*, 4479.
[41] N. B. Duong, V. M. Truong, Y. S. Li, C. L. Wang, H. Yang, *Energy Fuels* **2020**, *34*, 10050.
[42] Y. Chung, Y. Ahn, D. H. Kim, Y. Kwon, *J. Power Sources* **2017**, *337*, 152.
[43] M. Christwardana, D. H. Kim, Y. Chung, Y. Kwon, *Appl. Surf. Sci.* **2018**, *429*, 180.
[44] L. S. Y. Wong, S. Hossain, A. Ta, L. Weaver, C. Shaquer, A. Walker, J. Edvinsson, D. Rivas, H. Naas, A. Fawzi, A. Uhrenius, J. Lindberg, J. Johansson, P. Arvidsson, *Dig. Tech. Pap. – IEEE Int. Solid-State Circuits Conf.* **2004**, *47*, 2446.
[45] A. Caizzone, A. Boukhayma, C. Enz, in 2019 IEEE Int. Solid- State Circuits Conf., vol. *51*, IEEE, Piscataway, NJ **2019**, p. 290.
[46] C. Chen, G. Yu, Y. Huang, W. Cheng, Y. Li, Y. Sun, H. Ye, T. Liu, *Nat. Chem. Biol.* **2022**, *18*, 47.
[47] M. F. Sanad, V. S. N. Chava, A. E. Shalan, L. G. Enriquez, T. Zheng, S. Pilla, S. T. Sreenivasan, *ACS Appl. Mater. Interfaces* **2021**, *13*, 40731.
[48] Y. Zhou, D. Kong, X. Wang, G. Yu, X. Wu, N. Guan, W. Weber, H. Ye, *Nat. Biotechnol.* **2022**, *40*, 262.
[49] W. Lu, W. Bai, H. Zhang, C. Xu, A. M. Chiarelli, A. Vázquez-Guardado, Z. Xie, H. Shen, K. Nandoliya, H. Zhao, K. H. Lee, Y. Wu, D. Franklin, R. Avila, S. Xu, A. Rwei, M. Han, K. Kwon, Y. Deng, X. Yu, E. B. Thorp, X. Feng, Y. Huang, J. Forbess, Z. D. Ge, J. A. Rogers, *Sci. Adv.* **2021**, *7*, eabe0579.
[50] S. H. Byun, J. Y. Sim, Z. Zhou, J. Lee, R. Qazi, M. C. Walicki, K. E. Parker, M. P. Haney, S. H. Choi, A. Shon, G. B. Gereau, J. Bilbily, S. Li, Y. Liu, W. H. Yeo, J. G. McCall, J. Xiao, J. W. Jeong, *Sci. Adv.* **2019**, *5*, e.aay0418.
[51] H. Joo, Y. Lee, J. Kim, J. S. Yoo, S. Yoo, S. Kim, A. K. Arya, S. Kim, S. H. Choi, N. Lu, H. S. Lee, S. Kim, S. T. Lee, D. H. Kim, *Sci. Adv.* **2021**, *7*, abd4639.
[52] Y. Yang, R. Luo, S. Chao, J. Xue, D. Jiang, Y. H. Feng, X. D. Guo, D. Luo, J. Zhang, Z. Li, Z. L. Wang, *Nat. Commun.* **2022**, *13*, 6908.
[53] T. M. Jang, J. H. Lee, H. Zhou, J. Joo, B. H. Lim, H. Cheng, S. H. Kim, I. S. Kang, K. S. Lee, E. Park, S. W. Hwang, *Sci. Adv.* **2020**, *6*, eabc9675.
[54] R. Luo, Y. Liang, J. Yang, H. Feng, Y. Chen, X. Jiang, Z. Zhang, J. Liu, Y. Bai, J. Xue, S. Chao, Y. Xi, X. Liu, E. Wang, D. Luo, Z. Li, J. Zhang, *Adv. Mater.* **2023**, https://doi.org/10.1002/adma.202208395.
[55] D. Afanasenkau, D. Kalinina, V. Lyakhovetskii, C. Tondera, O. Gorsky, S. Moosavi, N. Pavlova, N. Merkulyeva, A. V. Kalueff, I. R. Minev, P. Musienko, *Nat. Biomed. Eng.* **2020**, *4*, 1010.
[56] A. Panov, Z. Orynbayeva, V. Vavilin, V. Lyakhovich, *Biomed Res. Int.* **2014**, *2014*, 472459.
[57] Z. Huang, L. Liu, J. Zhang, K. Conde, J. Phansalkar, Z. Li, L. Yao, Z. Xu, W. Wang, J. Zhou, G. Bi, F. Wu, R. J. Seeley, M. M. Scott, C. Zhan, Z. P. Pang, J. Liu, *Sci. Adv.* **2022**, *8*, eabn5345.
[58] H. Liu, M. M. Fergusson, J. J. Wu, I. I. Rovira, J. Liu, O. Gavrilova, T. Lu, J. Bao, D. Han, M. N. Sack, T. Finkel, *Sci. Signal.* **2011**, *4*, ra6.
[59] Y. Yuan, C. Zhu, Y. Wang, J. Sun, J. Feng, Z. Ma, P. Li, W. Peng, C. Yin, G. Xu, P. Xu, Y. Jiang, Q. Jiang, G. Shu, *Sci. Adv.* **2022**, *8*, eabn2879.
[60] P. Saeedi, I. Petersohn, P. Salpea, B. Malanda, S. Karuranga, N. Unwin, S. Colagiuri, L. Guariguata, A. A. Motala, K. Ogurtsova, J. E. Shaw, D. Bright, R. Williams, *Diabetes Res. Clin. Pract.* **2019**, *157*, 107843.
[61] X. Lin, Y. Xu, X. Pan, J. Xu, Y. Ding, X. Sun, X. Song, Y. Ren, P. F. Shan, *Sci. Rep.* **2020**, *10*, 14790.
[62] A. Ramanavicius, A. Kausaite, A. Ramanaviciene, *Biosens. Bioelectron.* **2008**, *24*, 761.
[63] C. Wang, E. Shim, H. K. Chang, N. Lee, H. R. Kim, J. Park, *Biosens. Bioelectron.* **2020**, *169*, 112652.
[64] A. Niiyama, K. Murata, Y. Shigemori, A. Zebda, S. Tsujimura, *J. Power Sources* **2019**, *427*, 49.
[65] S. Yin, Z. Jin, T. Miyake, *Biosens. Bioelectron.* **2019**, *141*, 111471.
[66] A. J. Gross, X. Chen, F. Giroud, C. Abreu, A. L. E. Goff, M. Holzinger, S. Cosnier, *ACS Catal.* **2017**, *7*, 4408.
[67] S. Cui, S. Gu, Y. Ding, J. Zhang, Z. Zhang, Z. Hu, *Talanta* **2018**, *178*, 788.
[68] S. Wang, X. Zhang, J. Huang, J. Chen, *Anal. Bioanal. Chem.* **2018**, *410*, 2019.
[69] G. Zeng, W. Li, S. Ci, J. Jia, Z. Wen, *Sci. Rep.* **2016**, *6*, 36454.
[70] P. Simons, S. A. Schenk, M. A. Gysel, L. F. Olbrich, J. L. M. Rupp, *Adv. Mater.* **2022**, *34*, 2109075.
[71] S. Padhi, A. K. Nayak, A. Behera, *Biomed. Pharmacother.* **2020**, *131*, 110708.
[72] V. Iacovacci, I. Tamadon, E. F. Kauffmann, S. Pane, V. Simoni, L. Marziale, M. Aragona, L. Cobuccio, M. Chiarugi, P. Dario, S. Del Prato, L. Ricotti, F. Vistoli, A. Menciassi, *Sci. Rob.* **2021**, *6*, eabh3328.
[73] M. Kim, H. Kim, Y. Lee, S. Lee, S. Kim, U. Lee, S. Jung, C. Park, J. Hong, J. Doh, D. Y. Lee, B. Kim, N. S. Hwang, *Sci. Adv.* **2021**, *7*, eabf7832.
[74] G. T. Dodd, S. J. Kim, M. Méquinion, C. E. Xirouchaki, J. C. Brüning, Z. B. Andrews, T. Tiganis, *Sci. Adv.* **2021**, *7*, eabf4100.
[75] G. Rossetti, J. A. Ermer, M. Stentenbach, S. J. Siira, T. R. Richman, D. Milenkovic, K. L. Perks, L. A. Hughes, E. Jamieson, G. Xiafukaiti, N. C. Ward, S. Takahashi, N. Gray, H. M. Viola, L. C. Hool, O. Rackham, A. Filipovska, *Sci. Adv.* **2021**, *7*, abi7514.
[76] Y. Jiang, T. Xia, L. Shen, J. Ma, H. Ma, T. Sun, F. Lv, N. Zhu, *ACS Catal.* **2021**, *11*, 2949.
[77] M. A. Bochenek, O. Veiseh, A. J. Vegas, J. J. McGarrigle, M. Qi, E. Marchese, M. Omami, J. C. Doloff, J. Mendoza-Elias, M. Nourmohammadzadeh, A. Khan, C. C. Yeh, Y. Xing, D. Isa, S. Ghani, J. Li, C. Landry, A. R. Bader, K. Olejnik, M. Chen, J. Hollister-Lock, Y. Wang, D. L. Greiner, G. C. Weir, B. L. Strand, A. M. A. Rokstad, I. Lacik, R. Langer, D. G. Anderson, J. Oberholzer, *Nat. Biomed. Eng.* **2018**, *2*, 810.
[78] A. J. Vegas, O. Veiseh, M. Gürtler, J. R. Millman, F. W. Pagliuca, A. R. Bader, J. C. Doloff, J. Li, M. Chen, K. Olejnik, H. H. Tam, S. Jhunjhunwala, E. Langan, S. Aresta-Dasilva, S. Gandham, J. J. McGarrigle, M. A. Bochenek, J. Hollister-Lock, J. Oberholzer, D. L. Greiner, G. C. Weir, D. A. Melton, R. Langer, D. G. Anderson, *Nat. Med.* **2016**, *22*, 306.

[79] A. J. Vegas, O. Veiseh, J. C. Doloff, M. Ma, H. H. Tam, K. Bratlie, J. Li, A. R. Bader, E. Langan, K. Olejnik, P. Fenton, J. W. Kang, J. Hollister-Locke, M. A. Bochenek, A. Chiu, S. Siebert, K. Tang, S. Jhunjhunwala, S. Aresta-Dasilva, N. Dholakia, R. Thakrar, T. Vietti, M. Chen, J. Cohen, K. Siniakowicz, M. Qi, J. McGarrigle, S. Lyle, D. M. Harlan, D. L. Greiner, et al., *Nat. Biotechnol.* **2016**, *34*, 345.
[80] D. Jacobs-Tulleneers-Thevissen, M. Chintinne, Z. Ling, P. Gillard, L. Schoonjans, G. Delvaux, B. L. Strand, F. Gorus, B. Keymeulen, D. Pipeleers, *Diabetologia* **2013**, *56*, 1605.
[81] J. T. McCluskey, M. Hamid, H. Guo-Parke, N. H. McClenaghan, R. Gomis, P. R. Flatt, *J. Biol. Chem.* **2011**, *286*, 21982.
[82] B. L. Furman, *Curr. Protoc.* **2021**, *1*, e78.